Expert Systems With Applications 249 (2024) 123651

Contents lists available at ScienceDirect

Expert Systems With Applications

journal homepage: www.elsevier.com/locate/eswa

A new emotional intelligent adaptive system for controlling the proposed sensor-less induction motor drive with dual stator winding based on a ten-switch converter in low speed range

Hojat Moayedirad[a,*], Mohammad Ali Shamsi-Nejad[b]

[a] Department of Electrical and Computer Engineering, Esfarayen University of Technology, Esfarayen, North Khorasan, Iran
[b] Faculty of Electrical and Computer Engineering, University of Birjand, Birjand, Iran

ARTICLE INFO

Keywords:
Dual stator
Ten-switch converter
Induction motor
Intelligent adaptive system
Sensor-less control

ABSTRACT

A dual stator winding induction motor (DSWIM) has two isolated three-phase windings in its stator, and its rotor is a usual squirrel cage type. In a sensor-less DSWIM drive, the standard and optimal operating mode in all operating speed ranges is the synchronous mode. Until now, researchers use the asynchronous mode to control it in the low speed range that is not the standard mode. But, this paper proposes a new intelligent model reference adaptive system (IMRAS) to control a DSWIM drive without the speed sensor based on a ten-switch converter in the low speed range. In the proposed intelligent sensor-less DSWIM drive, the rotor speed is estimated via an intelligent model as single and bi-objective functions. In the proposed IMRAS, the second objective increases the speed estimation accuracy at very low speeds. In this idea, the rotor speed error is used as data in the rotor speed estimation process. As a result, the convergence between estimated speed and reference speed in the proposed IMRAS is increased at zero and very low speeds. Also, in this paper, the power losses, the capital cost, and the number of switching elements in the converter are reduced via the concept of flux compensation and using a ten-switch converter. The intelligent proposed sensor-less DSWIM drive, unlike conventional methods, works in its standard operating mode (synchronous mode) and has a suitable performance in the low speed range. Hence, the converter power losses are significantly decreased. The suggested techniques are simulated in MATLAB software. The simulation of the proposed DSWIM drive system is performed under different scenarios of operating conditions and the obtained results approve the assumptions.

1. Introduction

In this study, the DSWIM has a usual squirrel cage rotor like an induction motor (IM) (Kumar & Hati, 2022) and a stator with two distinct three-phase windings with dissimilar numbers of poles. As shown in Fig. 1(a), each stator winding connects to an independent inverter. Due to having two independent separate stator windings, this motor has high reliability compared to IM. The modeling of a DSWIM was first presented by Munoz and Lipo (2000). Usually, the stator poles proportion are selected in the form of one to three. The normal operating mode in its drive is reached when the proportion of two frequencies supplying the *abc*1 and *abc*2 windings is equal to the proportion of the number of the stator poles (Munoz & Lipo, 2000). To have the maximum value of the torque per ampere proportion in its drive, it must work in its normal operating mode (Guerrero & Ojo, 2009). This is an essential condition for the DSWIM drive at low speed.

The control techniques of the drive in the three-phase induction motors are valid for DSWIM drive (Munoz & Lipo, 2000; Guerrero & Ojo, 2009). The most usual technique of the speed control in IMs drive is the vector control (Wang et al., 2022; Reddy & Loganathan, 2022; Moayedirad, Shamsi-Nejad, & Farshad, 2011; Moayedirad, Farshad & Shamsi-Nejad, 2012). The flux must is estimated in this control technique (Adamczyk & Kowalska, 2022; Moayedirad, Shamsi-Nejad, & Farshad, 2012). In this technique, due to the comparability of the stator resistance voltage drop with the stator input voltage, the rotor flux estimation has a significant sensitivity and fault in the low speed range, so disturbing the performance of the drive control system. Thus, in the low speed range, a suitable level of rotor flux is necessary. To solve the problem of an IM drive at low speed, Shamsi-Nejad, Farshad and Moayedirad (2010) proposed a neural method to generate suitable switching pulses for the

* Corresponding author.
E-mail addresses: hojatrad@gmail.com (H. Moayedirad), mshamsi@birjand.ac.ir (M.A. Shamsi-Nejad).

https://doi.org/10.1016/j.eswa.2024.123651
Received 22 April 2022; Received in revised form 1 December 2023; Accepted 8 March 2024
Available online 11 March 2024
0957-4174/

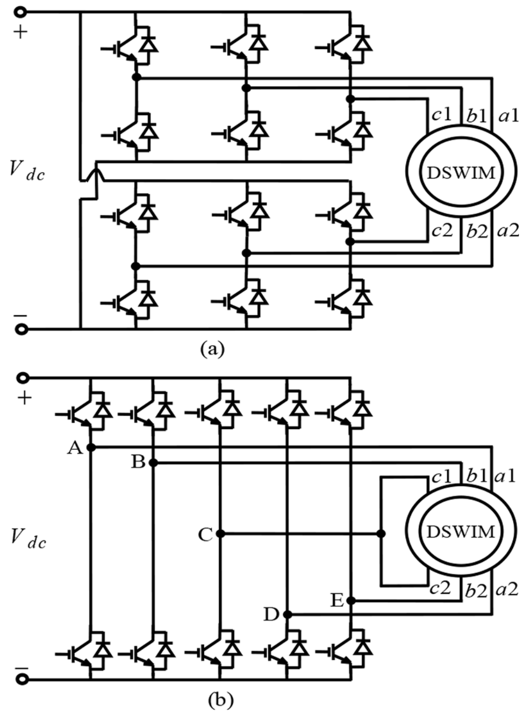

Fig. 1. The plane of the DSWIM drive with: a) Twelve-switch converter and b) The proposed ten-switch converter.

inverter unit. In this method, both the current and voltage of the reference of two phases of an IM drive are selected as the inputs of an artificial neural network. This network estimates the rotor flux based on data of currents and voltages of the reference, and its performance is acceptable in the low and high speed range. But the performance of this neural method has not been tested in the sensor-less mode.

Moaveni, Masoumi and Rahmani (2023), Yoo, Lee, Sul and Baloch (2020), Zhao et al. (2021), and Luo et al. (2020) estimated the stator resistance to improve the speed estimation of an IM drive in the low speed range. By estimating the accurate value of the stator resistance, a proper level of the flux is provided. Zerdali (2020), Yildiz, Barut and Zerdali (2020) and Özkurt and Zerdali (2022) proposed several kinds of the reformed extended Kalman filter (EKF) to improve estimating the flux and torque. These methods work via the mechanism of the algorithm repeat. In these algorithms, the computation time is high. Stender, Wallscheid and Böcker (2021) proposed an adaptive Kalman filter based on a particle swarm optimization to control an induction motor drive. Due to the high repetition of the algorithm, PSO and EKF are inappropriate for online estimation in real time, particularly for fast-speed variations, which makes poor accuracy in the low speed range. Zhao et al. (2021) estimated the rotor and stator resistances to improve the IM drive performance at low speeds. By estimating the stator resistance, the proper rotor flux level is established and the motor drive control system traces the low speeds acceptably.

Moayedirad, Shamsi-Nejad and Farshad (2012) proposed an automatic compensator of the rotor flux to improve estimating the rotor flux in the low speed range of the IM drive. This method has completely solved the issue of estimating flux in the low speed range of an IM drive. Unlike the proposed methods by Moaveni et al. (2023), Yoo, Lee, Sul and Baloch (2020), Zhao et al. (2021), and Luo et al. (2020), in this technique, there is no need to estimate the stator resistance.

In summary, the disadvantages of the conventional approaches of the sensor-less DSWIM drive are as following cases:

1. At low speeds, the conventional approaches control the DSWIM drive in the asynchronous mode. But, the appropriate efficiency and the trapezoidal normal form of the total rotor flux in a DSWIM drive are achieved when it is controlled in the synchronous mode.
2. In the synchronous mode, it is difficult to estimate the rotor speed at low speeds. In other approaches, researchers commonly drive a DSWIM in the asynchronous mode to solve this issue. In this mode, the efficiency of the DSWIM drive is not appropriate.
3. A sensor-less DSWIM drive normally has two independent converters (in total 12 IGBT/Diode switches). So, in terms of the economy, managing energy, and increasing reliability, it is essential to decrease the number of converter switches.

The industry society could use the best induction motor available technology to minimize the use of energy in inverter unit and sensors, and also to increase the reliability of an induction motor based on a sensor-less DSWIM drive. A DSWIM has an important feature which is the existence of two isolated stator windings. So far, in the conventional method, this hardware attribute is utilized to solve the problem of the rotor speed control in the low speed range. In proposed method by Munoz and Lipo (2000), the *abc*1 winding of a DSWIM is excited by a free constant frequency and the *abc*2 winding is excited via an adjustable frequency. Unlike the *abc*1 winding, the *abc*2 winding can generate negative and positive torques. Therefore, by imposing the *abc*1 three-phase winding to feed at a free constant frequency, the DSWIM avoids its normal operational mode (asynchronous mode). The suggested methods by Wu, Ojo and Sastry (2007) and Ojo and Wu (2007) are based on the suggested method by Munoz and Lipo (2000).

In a DSWIM drive, usual control methods result in the loss of optimal energy management in the low speed range. The suitable efficiency in a DSWIM drive is achieved when it operates in its normal mode (Guerrero & Ojo, 2009). The inverter unit of a DSWIM drive has in total twelve switches. Decreasing the number of converter switches can decrease the cost of the inverter unit (Sabarad & Kulkarni, 2020; Mahato, Majumdar, & Jana, 2020). A ten-switch converter can control two motors separately as reported by Sabarad and Kulkarni (2020), Jing and Zhou (2020), Choi et al. (2023), Geng et al. (2022), and Wang et al. (2020). In the low speed range, the core losses of an IM are not considerable (Novotny and Lipo, 1997). Therefore, to have higher energy efficiency, it is important to decrease the power losses in the converter with the lowest cost. In the proposed sensor-less DSWIM drive, one of the main objectives is to reduce the power losses of the converter unit in the low speed range using the proposed models.

The challenges in a DSWIM drive are as following cases:

1. Challenge 1: Due to the low flux level, a DSWIM drive, in its normal operating mode, cannot correctly trace low speeds via conventional control methods. To solve this issue, researchers control the DSWIM drive in the asynchronous mode. In this operating mode, the proper rotor flux level is established and the DSWIM drive control system traces the low speeds acceptably. But the appropriate efficiency and the trapezoidal usual form of the total rotor flux in a DSWIM drive are achieved when it is controlled in the synchronous mode (Guerrero and Ojo, 2009). Thus, at low speeds, researchers control a DSWIM drive acceptably but with inappropriate efficiency.
2. Challenge 2: It is difficult to estimate the rotor speed at low speeds. In the conventional MRAS, researchers commonly estimate the stator resistance (R_s) to solve this issue. The error of the stator resistance estimation is relatively high at low speeds.
3. Challenge 3: As shown in Fig. 1, unlike an IM sensor-less drive, a DSWIM sensor-less drive has two independent converters. So, in terms of the economy, managing energy, and increasing reliability, it is essential to decrease the number of converter switches. The ten-switch converter has the advantages of small size and low cost.

In this paper, the novelty and contribution of the proposed models to solve all three challenges are as follows:

1. To solve Challenge 1, an automatic compensator of the rotor flux is used to improve estimating the rotor flux in the low speed and the sensor-less DSWIM drive can be controlled in its normal operating mode (synchronous mode) in the low speed range.
2. To solve Challenge 2, the new intelligent model reference adaptive system (IMRAS) is proposed to estimate the rotor speed in the proposed DSWIM drive system via the proposed ideas in the low speed range. In this paper, IMRAS is modeled as a single and bi-objective function. In the bi-objective idea, the information of the reference speed is involved in the speed estimate calculations via the rotor speed error. As a result, the convergence between estimated speed and reference speed in the proposed IMRAS is increased at very low speeds. In this method, unlike conventional methods, it is not need to estimate the stator resistance. In proposed method, the brain emotional learning is very suitable algorithm because does not act based on algorithm iteration. Thus, its computational time is short.
3. To solve Challenge 3, a ten-switch converter is proposed to feed the proposed sensor-less DSWIM drive. The proposed plan for a DSWIM drive is shown in Fig. 1(b). In this study, the decrease of switches in the converter of the sensor-less DSWIM drive can be reached using a ten-switch converter. The superiority of utilizing this converter in the sensor-less DSWIM drive is the power losses reduction and also the capital cost in the inverter unit.

This paper is organized as follows: The motor model is presented in Section 2. The presented model for the sensor-less DSIM drive and the speed estimation using IMRAS are explained in Sections 3. The proposed ten-switch inverter for controlling the sensor-less DSWIM drive is explained in Section 4, and finally, results and conclusion are presented in Sections 5 and 6, respectively.

2. Motor model

In this paper, the DSWIM has a typical squirrel cage rotor and a stator with two three-phase windings. The stator windings are wounded with dissimilar numbers of the poles. The DSWIM is like two three-phase IMs that are mechanically coupled through a shaft. Figs. A1 and A2 show the equivalent circuit and a shape of the DSWIM with the 2-pole and 6-pole stator windings (see Appendix A). The stator and rotor voltages of a DSWIM in the d-q form are defined in a complex form as Eq. (1) (Munoz and Lipo, 2000; Ojo and Wu, 2008).

$$\begin{bmatrix} V_{qdsi} \\ V_{qdri} \end{bmatrix} = \begin{bmatrix} r_{si} & 0 \\ 0 & r_{ri} \end{bmatrix} \begin{bmatrix} i_{qdsi} \\ i_{qdri} \end{bmatrix} + \begin{bmatrix} \rho - j\omega & 0 \\ 0 & \rho - j(\omega - \omega_{ri)} \end{bmatrix} \begin{bmatrix} \lambda_{qdsi} \\ \lambda_{qdri} \end{bmatrix} \tag{1}$$

where i shows the number of stator windings. In a common reference frame, ω show the electrical rotating speed; ω_{ri} is rotor electrical speed; V_{qdri} and V_{qdsi} are rotor and stator voltages in d-q form, respectively; i_{qdri} and i_{qdsi} are rotor and stator currents in d-q form, respectively; λ_{qdri} and λ_{qdsi} are rotor and stator flux linkages in d-q form, respectively; r_{ri} and r_{si} show the value of rotor and stator resistances, respectively, and ρ is a derivative operator. The stator and rotor currents are identified as Eq. (2).

$$\begin{bmatrix} i_{qdsi} \\ i_{qdri} \end{bmatrix} = \begin{bmatrix} L_{ri}/D_i & -L_{mi}/D_i \\ -L_{mi}/D_i & L_{si}/D_i \end{bmatrix} \begin{bmatrix} \lambda_{qdsi} \\ \lambda_{qdri} \end{bmatrix} \tag{2}$$

where L_{si}, L_{ri}, and L_{mi} are the stator, rotor, and magnetizing inductances, respectively, and $D_i = L_{si}\, L_{ri}$ - $L^2{}_{mi}$. By replacing Eq. (2) into Eq. (1), the voltage equations convert as Eq. (3). The generated electromagnetic torque (T_{ei}) in each stator three-phase winding is defined as Eq. (4) in a complex variable form.

$$\begin{bmatrix} V_{qdsi} \\ V_{qdri} \end{bmatrix} = \begin{bmatrix} \rho - j\omega + r_{si}L_{ri}/D_i & -r_{si}L_{mi}/D_i \\ -r_{ri}L_{mi}/D_i & \rho - j(\omega - \omega_{ri}) + r_{ri}L_{si}/D_i \end{bmatrix} \begin{bmatrix} \lambda_{qdsi} \\ \lambda_{qdri} \end{bmatrix} \tag{3}$$

$$T_{ei} = (3/2)(P_i/2)\mathrm{Im}(\lambda_{qdsi}.\, i^*_{dqsi}) \tag{4}$$

where P_i shows the pole number of windings and $V_{qdri} = 0$. In a DSWIM, the total torque (T_e) is the sum of produced torques using both $abc1$ and $abc2$ windings, which is expressed as Eq. (5) (Munoz & Lipo, 2000). Rotor electrical speeds ω_{r1} and ω_{r2} are expressed as Eq. (6) (Ojo & Wu, 2007).

$$\begin{aligned} T_e = T_{e1} + T_{e2} = (3/2)(P_1/2)\mathrm{Im}\left(\lambda_{qds1}\ i^*_{dqs1}\right) \\ +(3/2)(P_2/2)\mathrm{Im}\left(\lambda_{qds2}\ i^*_{dqs2}\right) \end{aligned} \tag{5}$$

$$\omega_{ri} = (P_i/2)\omega_r \tag{6}$$

where ω_r is the rotor mechanical speed (ω_r). The air gap flux linkage is defined as Eq. (7).

$$\lambda_{qdmi} = L_{mi}i_{qdsi} + L_{mi}i_{qdri} \tag{7}$$

The currents are omitted by replacing Eq. (2) into Eq. (7). Thus, Eq. (7) is rephrased as Eq. (8).

$$\lambda_{qdmi} = \frac{L_{lri}L_{mi}}{D_i}\lambda_{qdsi} + \frac{L_{lsi}L_{mi}}{D_i}\lambda_{qdri} \tag{8}$$

The total air gap flux linkage is the sum of the two distinct air gap flux linkages that is defined as Eq. (9).

$$\begin{aligned} \lambda_{qdm} = (L_{lr1}L_{m1}/D_1)\lambda_{qds1} + (L_{ls1}L_{m1}/D_1)\lambda_{qdr1} \\ +(L_{lr2}L_{m2})/D_2\lambda_{qds2} + (L_{ls2}L_{m2}/D_2)\lambda_{qdr2} \end{aligned} \tag{9}$$

The motor mechanical equation is defined by Eq. (10).

$$\begin{aligned} \rho\omega_r = (K_{e1}/J)\left(\lambda_{dr1}I_{qs1} - \lambda_{qr1}I_{ds1}\right) \\ +(K_{e2}/J)\left(\lambda_{dr2}I_{qs2} - \lambda_{qr2}I_{ds2}\right) - T_L/J \end{aligned} \tag{10}$$

where J shows the inertia coefficient, K_{e1}=(3P_1/4)(L_{m1}/L_{r1}), and K_{e2}=(3P_2/4)(L_{m2}/L_{r2}). The low-pole and high-pole number windings are referred to as $abc1$ and $abc2$, respectively. In this motor, the relative magnitude of the harmonic components depends on the amount of phase shift between the 2-pole and 6-pole MMFs. As it is analyzed by Munoz and Lipo (2000), the worst scenario occurs when the peaks of the two MMF distributions coincide in time and space (180° phase shift).

3. Presented model for the sensor-less DSWIM drive

3.1. Modeling the control system of sensor-less DSWIM drive

In the voltage model, the control signals are generated as Eqs. (11)–(17) (Bose, 2002).

$$\varphi^s_{dqsi} = \int \left(v^s_{dqsi} - R_{si}i^s_{dqsi}\right)dt \tag{11}$$

$$\varphi^s_{qdmi} = \varphi^s_{qdsi} - L_{lsi}i^s_{qdsi} \tag{12}$$

$$\varphi^s_{dqri} = (L_{ri}/L_{mi})\varphi^s_{dqmi} - L_{lri}i^s_{dqsi} \tag{13}$$

$$T_{ei} = (3P_i/4)\left(\varphi^s_{dsi}i^s_{qsi} - \varphi^s_{qsi}i^s_{dsi}\right) \tag{14}$$

$$\varphi_{ri} = \sqrt{\left(\varphi^s_{qri}\right)^2 + \left(\varphi^s_{dri}\right)^2} \tag{15}$$

$$\cos\theta_{ei} = \varphi^s_{dri}/\varphi_{ri} \tag{16}$$

$$\sin\theta_{ei} = \varphi^s_{qri}/\varphi_{ri} \tag{17}$$

where φ^s_{dqsi}, φ^s_{dqri}, and φ^s_{dqmi} are stator, rotor and air gap fluxes in d-q form, respectively; L_{lsi} and L_{lri} are stator and rotor leakage inductances, respectively. Fig. 2 shows a plan of the proposed sensor-less DSWIM drive based on the proposed IMRAS method. In this figure, T_r, V_{dc}, and $\varphi^*_{r1\_m}$ are the rotor time constant, the voltage of the dc link, and the reference rotor flux, respectively; i^*_a, i^*_b, i^*_x, and i^*_y are stator reference currents; $\widehat{\omega}_r$ and $\Delta\omega_r$ are the estimated speed and the speed error, respectively; K_1 and K_2 are the torque sharing factor and the flux coefficient, respectively. To avoid deep saturation and reduce motor iron losses, Munoz and Lipo (2000) calculated the correct value of the flux coefficient (K_2 =0.662). In the standard mode of a DSWIM drive, the value of the torque sharing factor is 0< K_1 < 1. The rotor fluxes are estimated from air gap fluxes as Eq. (13). Similarly, air gap fluxes (φ^s_{dmi} and φ^s_{dmi}) are estimated from stator fluxes as Eq. (13). The stator flux is achieved by Eq. (11). The pure integrator is modeling as the presented algorithm by Hu and Wu (1998).

3.2. Modeling flux compensator

The voltage model works based on the estimation of unit vectors and the rotor flux. In the low speed range, the flux is low and is not able to produce the demand torque to drive the motor. Consequently, the actual torque (T_{ei}) is continually smaller than the reference torque (T_{ei}*). In this study, the flux rotor is compensated via a PI controller whose input is ΔT_e (Moayedirad, Farshad & Shamsi-Nejad, 2012). This technique creates a flux suitable level and compensates the unsuitable effect of the voltage drop on the stator resistance.

3.3. Modeling speed estimator using IMRAS

In the low speed range, there are two issues in a classic MRAS:

1. In the low speed range, due to the existence of the pure integrations and low flux level in the reference model (see Eq. (11)), it is difficult to estimate the rotor speed (Reddy et al., 2020; Bose, 2002). To solve this issue, researchers commonly estimate R_s (Moaveni et al., 2023; Sun et al., 2021; Yoo, Lee, Sul & Baloch, 2020). The process of estimating R_s increases the computational time in MRAS.

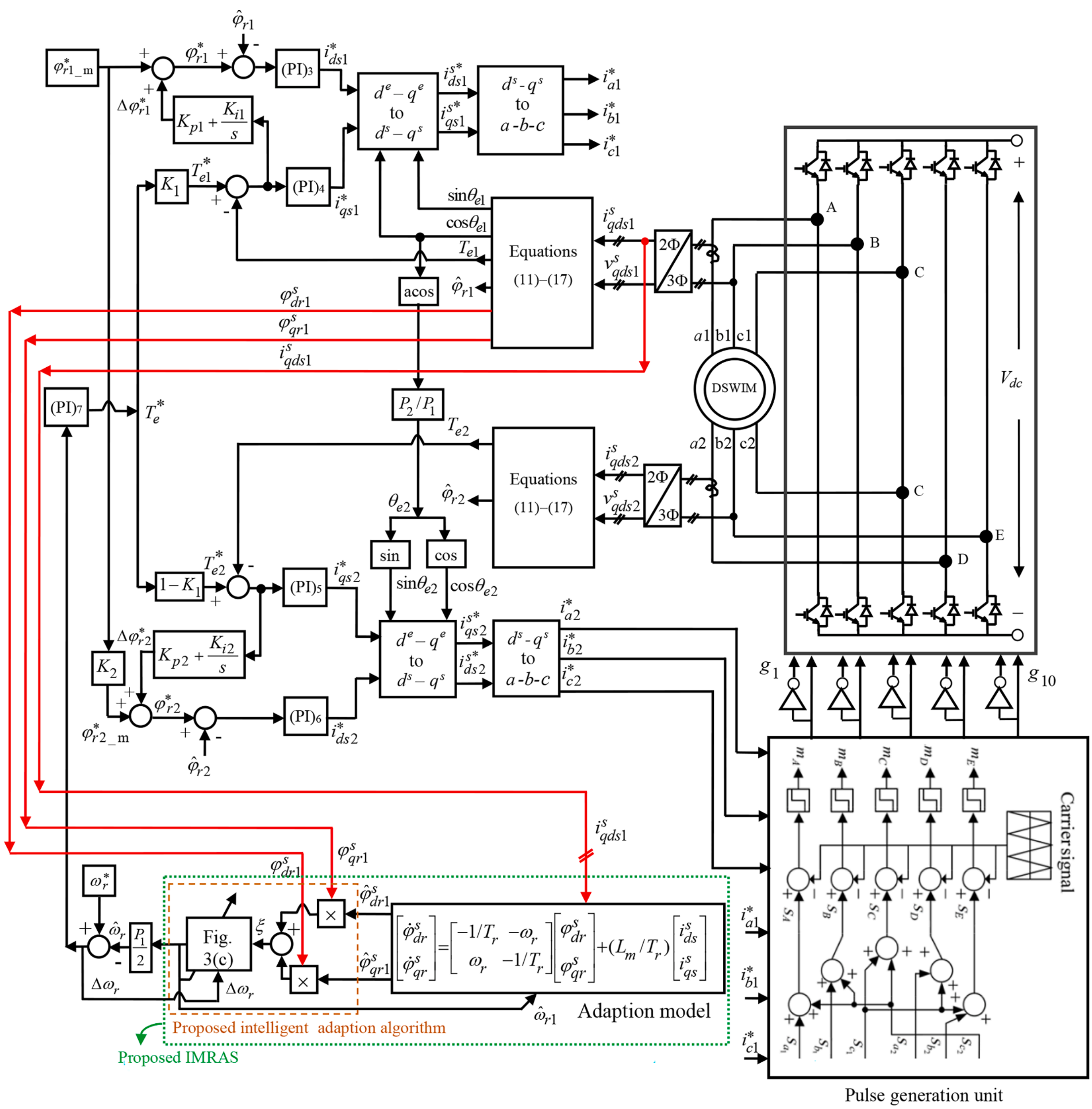

Fig. 2. Plan of the proposed model for controlling the sensor-less DSWIM drive using ten-switch inverter.

2. In the conventional adaptive algorithm of MRAS, tuning coefficients of proportional (k_p) and integral (k_i) are imperative to abstain a high accuracy in the sensor-less DSWIM drive.

In the proposed IMRAS:

1. An integration algorithm introduced by Hu and Wu (1998) is used instead of the pure integrator, and the flux in the reference model is automatically compensated based on the rotor flux compensator without estimating the stator resistance.
2. k_p and k_i coefficients in the adaptive algorithm are automatically tuned using the proposed bi-objective emotional intelligent algorithm.

In the proposed IMRAS, the first objective is $\xi \rightarrow 0$ to balance fluxes ($\varphi^s_{dr} = \widehat{\varphi}^s_{dr}$ and $\varphi^s_{qr} = \widehat{\varphi}^s_{qr}$). To have an exact and true estimation of the rotor speed in the low speed range, the rotor speed error ($\Delta\omega_r \rightarrow 0$) is expressed as another objective in the intelligent adaptive algorithm. The structure of an emotional intelligent controller is simple and has no complexity, so it acts in real time and is suitable for online applications. Emotional models have successful performance in control systems (Farshad & Lucas, 2006; Rouhani et al., 2007; Savarapu, Qutubuddin, & Narri, 2022). In this study, modeling adaptive algorithm is performed based on a computational model proposed by Moren and Balkenius (2000) to extend a new intelligent model for the proposed IMRAS. Fig. 3 (a) shows the Amygdala unit and Orbitofrontal cortex unit (AU and OCU) in the brain of a human. Fig. 3(b) shows the plan of a brain emotional learning model (BELM) (Moren & Balkenius, 2000).

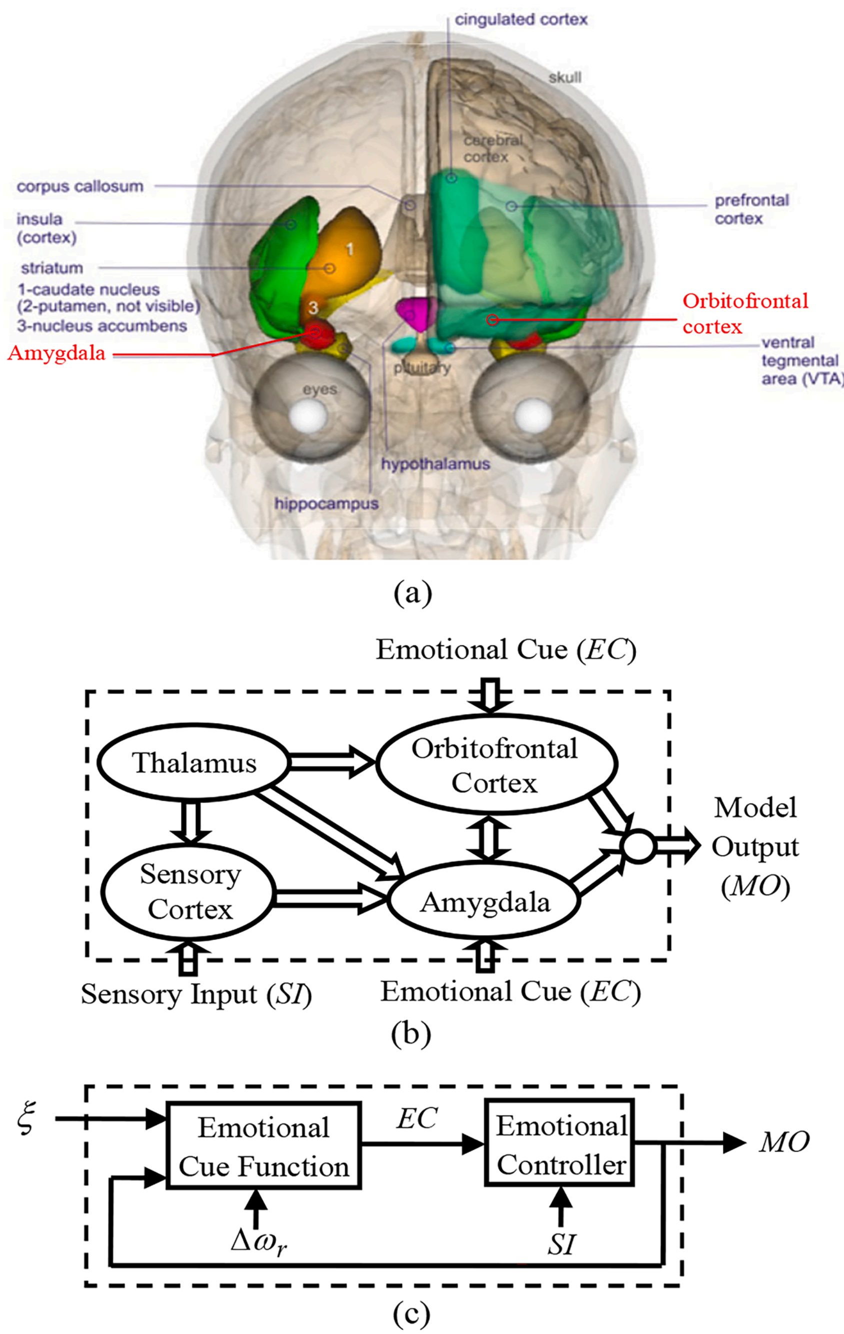

Fig. 3. a) AU and OCU in the main of a human (Blanchard et al., 2009), b) A plane of the BELM method (Moren & Balkenius, 2000), and c) Proposed intelligent structure for modeling PI controller using the BELM in the adaptive algorithm as the bi-objective function ($\xi \rightarrow 0$ and $\Delta\omega r \rightarrow 0$).

Equations (18)–(32) define the proposed model for the intelligent PI controller (Farshad & Lucas, 2006). The learning operation is performed in AU. OCU is used to reform the actions and AU inappropriate reactions. Equations (18), (19), and (20) show the response of BELM (*MO*) to sensory input (*SI*) and emotional cue (*EC*).

$$MO = AO - OCO \tag{18}$$

$$A\,O = G_a.\,SI \tag{19}$$

$$OCO = G_{oc}.\,SI \tag{20}$$

where *AO*, *OCO*, G_a, and G_{oc} show the outputs and gains of AU and OCU, respectively. Equations (21) and (22) express the training law in AU and OCU, respectively.

$$\Delta G_a = C_1.\max(0\ ,\ EC - AO) \geqslant 0 \tag{21}$$

$$\Delta G_{oc} = C_2.(MO - EC) \tag{22}$$

where C_1 and C_2 are training coefficients of AU and OCU, respectively. According to operator "max" in Eq. (21), AU unable ignore what that has been learning before, so the gain of AU always is rising. The OCU gain variation is free to reform well the inappropriate actions of AU (Farshad & Lucas, 2006). By combining Eqs. (18)–(20), MO can be written as Eq. (23) that in the proposed IMRAS *SI* is expressed as Eq. (24).

$$MO = (G_a - G_{oc}).\,SI = G(SI, EC, \ldots).\,SI \tag{23}$$

$$SI = k_p.\xi + k_i.\int_0^t \xi\,dt,\quad \xi = \widehat{\varphi}^s_{dr}\,\varphi^s_{qr} - \widehat{\varphi}^s_{qr}\,\varphi^s_{dr} \tag{24}$$

For obtaining $G_a(t)$, Eq. (21) is rewritten as Eq. (25).

$$\frac{G_a(t+\Delta t) - G_a(t)}{\Delta t} = C_1^{'}.\max\left(0, EC(t) - AO(t)\right) \tag{25}$$

where $C_1^{'}$ is the learning coefficient in AU ($C_1^{'} = C_1/\Delta t$). $G_a(t)$ is achieved by Eq. (26) as Eq. (27). For obtaining $G_{oc}(t)$, Eq. (22) is rewritten as Eq. (28).

$$\frac{d}{dt}G_a(t) = C_1^{'}.\max(0,\ EC(t) - AO(t)) \tag{26}$$

$$G_a(t) = C_1^{'}\int_0^t \max(0, EC(t) - AO(t))\,dt\ +\ G_a(0) \tag{27}$$

$$\frac{G_{oc}(t+\Delta t) - G_{oc}(t)}{\Delta t} = C_2^{'}(MO(t) - EC(t)) \tag{28}$$

where $C_2^{'}$ is the learning coefficient in OCU ($C_2^{'} = C_2/\Delta t$). $G_{oc}(t)$ is achieved by Eq. (29) as Eq. (30).

$$\frac{d}{dt}G_{oc}(t) = C_2^{'}(MO(t) - EC(t)) \tag{29}$$

$$G_{oc}(t) = C_2^{'}\int_0^t (MO(t) - EC\,(t))\,dt\ +\ G_{oc}(0) \tag{30}$$

EC is expressed using the required purposes (Farshad & Lucas, 2006). In this study, it is expressed as Eqs. (31) and (32).

$$\text{Single-objective } (\xi \to 0):\ EC = a_{ec1}.\,\xi + a_{ec2}.MO \tag{31}$$

$$\begin{gathered}\text{Bi-objective } (\xi \to 0 \text{ and } \Delta\omega_r \to 0):\\ EC = a_{ec1}.\,\xi + a_{ec2}.MO + a_{ec3}.\,\Delta\omega_r\end{gathered} \tag{32}$$

where $\Delta\omega_r$ is the rotor speed error; and a_{ec1}, a_{ec2}, and a_{ec3} are *EC* function input coefficients. Fig. 3(c) shows the proposed intelligent PI controller. It is difficult and sensitive to balance fluxes in the low speed range. Thus, in this study, IMRAS is modeled as the single ($\xi \to 0$) and bi-objective ($\xi \to 0$ and $\Delta\omega_r \to 0$). In modeling single-objective ($\xi \to 0$), the rotor speed is estimated only by balancing the components of the rotor flux. The main target in the DSWIM drive is to decrease the speed error to zero ($\Delta\omega_r = \omega_r^* - \widehat{\omega}_r \to 0$). This target is chosen as the second target in the PI controller of the proposed IMRAS. In other words, the amount of $\Delta\omega_r$ has straight participated in estimating speed. Consequently, the convergence between $\widehat{\omega}_r$ and ω_r^* is increased at very low speeds which in turn decreases the speed estimation fault. In the proposed IMRAS, the brain emotional learning is an appropriate method to adjust the PI controller coefficients and unlike other methods, the k_p and k_i coefficients are adjusted online. Thus, its calculation time duration is very short. The most important feature of the proposed IMRAS model is that the data of the reference speed (ω_r^*) involve in the speed estimate calculations via $\Delta\omega_r$. As a result, the convergence between $\widehat{\omega}_r$ and ω_r^* in the proposed IMRAS is increased at very low speeds.

3.4. Sensitivity analysis of the proposed model

The proposed model for controlling sensor-less DSWIM drive is based on compensating the rotor flux and has inherent robustness to R_s variation, but estimating $\widehat{\varphi}^s_{dr}$ and $\widehat{\varphi}^s_{qr}$ in IMRAS are dependent on R_r variation as Eqs. (33) and (34).

$$\widehat{\varphi}^s_{qr} = \left(i^s_{ds}L_mR_r\Big/L_r - \rho\widehat{\varphi}^s_{qr} - \widehat{\varphi}^s_{qr}R_r\Big/L_r\right)\Big/\widehat{\omega}_r \tag{33}$$

$$\widehat{\varphi}^s_{dr} = -\left(i^s_{qs}L_mR_r\Big/L_r - \rho\widehat{\varphi}^s_{dr} - \widehat{\varphi}^s_{dr}R_r/L_r\right)\Big/\widehat{\omega}_r \tag{34}$$

In Eqs. (33) and (34), $\widehat{\varphi}^s_{dr}$ and $\widehat{\varphi}^s_{qr}$ are estimated by the adaptive model. Kowalska and Dybkowski (2010) considered that the robustness of the MARS to R_r changes depends on the amount of k_p and k_i coefficients in the adaptation algorithm. These coefficients must be updated to make the control system resistant to rotor resistance changes. In the proposed intelligent model, k_p and k_i coefficients in the adaptation algorithm are tuned based on the BELM as a bi-objective function. In the proposed IMRAS, BELM is an appropriate technique to adjust k_p and k_i coefficients. According to Eqs. (33) and (34), the normalized sensitivity functions of $\widehat{\varphi}^s_{dr}$ and $\widehat{\varphi}^s_{qr}$ to R_r changes ($S^{\widehat{\varphi}^s_{dr}}_{R_{r1}}$ and $S^{\widehat{\varphi}^s_{qr}}_{R_{r1}}$) in the adaptive model of the proposed IMRAS can be expressed as Eqs. (35) and (36), respectively.

$$S^{\widehat{\varphi}^s_{qr1}}_{R_{r1}} = \frac{\partial\widehat{\varphi}^s_{qr1}\Big/\widehat{\varphi}^s_{qr1}}{\partial R_{r1}/R_{r1}} = (R_{r1}\Big/(L_{r1}\widehat{\varphi}^s_{qr1}\widehat{\omega}_r))\left(L_{m1}i^s_{ds1} - \widehat{\varphi}^s_{dr1}\right) \tag{35}$$

$$S^{\widehat{\varphi}^s_{dr1}}_{R_{r1}} = \frac{\partial\widehat{\varphi}^s_{dr1}/\widehat{\varphi}^s_{dr1}}{\partial R_{r1}/R_{r1}} = (R_{r1}/(L_{r1}\widehat{\varphi}^s_{dr1}\widehat{\omega}_r))\left(\widehat{\varphi}^s_{qr1} - L_{m1}i^s_{qs1}\right) \tag{36}$$

where $\widehat{\omega}_r$ is the estimated speed via bi-objective IMRAS. In Section 6, the sensitivity analysis of $\widehat{\varphi}^s_{dr}$ and $\widehat{\varphi}^s_{qr}$ to R_r changes are considered (see Fig. 6).

3.5. Stability analysis of the proposed model

The proposed intelligent adaption algorithm requires several design parameters that it is possible to seem a drawback. Anyway, the intelligent algorithm requires several initial values to create the initial value of gains and signals in the brain emotional algorithm. The appropriate initial values range can be chosen with the help of the stability analysis and problem constraints. As reported by Farshad and Lucas (2006), the effect of initial values of the brain learning algorithm parameters in the suitable range are on the system transient response.

The design of the model reference adaptive system is based on the Hyperstability concept (Landau, 1979), which in the main relevancies the stability attributes of a class of feedback systems as demonstrated in Fig. A4 (see Appendix A). Such a control system is said to be globally stable if the following two conditions hold:

1. The linear feedforward block of the transfer function should be positive real.

2. The nonlinear feedback block satisfies Popov's integral inequality of Eq. (37)

$$\mu(0,\ t_1) = \int_0^{t_1} \alpha^T \beta dt \geqslant -\gamma^2 \qquad \forall t_1 > 0 \tag{37}$$

where α and β are the input and output vectors of the feedback block, respectively, and γ is a finite constant.

In the forward path, the transfer function is based on the voltage model of the DSWIM. Therefore, it can be shown that the forward path is indeed strictly positive real (Schauder, 1992). For stability analysis of the proposed observer, according to Eqs. (38)–(41), the equivalent nonlinear feedback system of the model reference adaptive system observer can be described as Fig. A4 (see Appendix A). Based on the basic equations of MRAS, the input of the adaptation algorithm (ξ) is defined as Eq. (38).

$$\xi = X - Y = A_1 - \widehat{\omega}_r(\xi, t)A_2 \tag{38}$$

where X and Y are the output vectors of reference and adjustable models, respectively, and $\widehat{\omega}(\xi,t)$, A_1, and A_2 are defined as Eqs. (39)–(41), respectively (Bose, 2002).

$$\widehat{\omega}_r(\xi, t) = \left(k_p + k_i/s\right)\alpha \tag{39}$$

$$A_1 = v_{qs}\, i_{ds} - v_{ds}\, i_{qs} - (R_r/L_r)\left(i_{qs}/i_{qs}\right)A_2 \tag{40}$$

$$A_2 = \partial L_s\left(i_{ds}^2 + i_{qs}^2\right) + i_{ds}^2\left(L_m^2/L_r\right) \tag{41}$$

In Fig. A3(b) (see Appendix A), β is defined as Eq. (42).

$$\beta = -A_1 + A_2\, \widehat{\omega}_r(\xi, t) \tag{42}$$

By substituting Eq. (42) in Eq. (37), the inequality becomes as Eq. (43).

$$\int_0^{t_1} (-\alpha A_1 + \alpha^2 A_2\left(k_p + k_i/s\right) + \alpha A_2 \widehat{\omega}_r(\xi, t) dt) \geqslant -\gamma^2 \tag{43}$$

According to Eq. (44), which is a well-known inequality, it can be shown that Eq. (43) is satisfied.

$$\int_0^{t_1} \frac{d}{dt} f(t) k f(t) dt \geqslant -0.5 k f(0)^2 \qquad \forall k > 0 \tag{44}$$

Thus, a PI controller is adequate to satisfy Popov's hyperstability theory. In this paper, k_p and k_i coefficients in the adaptation algorithm are updated based on an emotional learning algorithm. In the emotional intelligent PI controller, the OCU gain variation is free to reform well the inappropriate actions of AU. Thus, the OCU gain behavior is important in the stability analysis. By substituting Eq. (32) in Eq. (22), the ΔG_{OC} is rewritten as Eq. (45).

$$\Delta G_{oc} = C_2.((1 - a_{ec2})MO - a_{ec1}.\xi - a_{ec3}.\Delta\omega_r) \tag{45}$$

According to Eqs. (22), (23), and (45), it is clear that the dynamic of the OCU gain is faster than the dynamics of other parameters of the closed-loop system (Farshad & Lucas, 2006). Thus, ξ, $\Delta\omega_r$, and SI signals are assumed constant in small-signal stability analysis ($\delta_\xi = 0, \delta_{\Delta\omega_r} = 0$). The form small-signal of MO and Eq. (45) are defined as Eqs. (46) and (47), respectively.

$$\delta_{MO} = -\delta_{G_{oc}}.SI \tag{46}$$

$$\begin{aligned}\delta_{\Delta G_{oc}} &= C_2.\left((1 - a_{ec2}).\delta_{MO} - a_{ec1}.\delta_\xi - a_{ec3}.\delta_{\Delta\omega_r}\right)\\ &\approx C_2((1 - a_{ec2}).\delta_{MO})\end{aligned} \tag{47}$$

By substituting Eq. (46) in Eq. (47), $\delta_{\Delta G_{oc}}$ is defined as Eq. (48).

$$\delta_{\Delta G_{oc}} \approx -C_2(1 - a_{ec2}).\delta_{G_{oc}}.SI \tag{48}$$

$\delta_{\Delta G_{oc}}$ is rewritten as Eq. (49) if $\delta_{\Delta G_{oc}} \triangleq y$ and $\delta_{G_{oc}} \approx \frac{dy}{dt}$.

$$\frac{dy}{dt} + C_2(1 - a_{ec2}).SI.y = 0 \tag{49}$$

By taking the Laplace transform of Eq. (49), the Laplace transform of small variations of the OCU gain ($Y(s)$) is defined as Eq. (50).

$$Y(S) = \frac{1}{S + C_2(1 - a_{ec2}).SI} \tag{50}$$

According to Eq. (50):

1. If $a_{ec2} \geq 1$, the feedback in the inner loop of G_{OC} gain adjustment becomes positive. In other words, changes G_{OC} and ΔG_{OC} are aligned, so that in $a_{ec2} = 1$, $Y(s)$ will have a pole at the coordinate origin and is ready to diverge. If $a_{ec2} > 1$, $Y(s)$ has an unstable real pole. Thus, $Y(s)$ (and subsequently the closed-loop system becomes unstable. The instability caused by positive feedback can be eliminated by applying limiters to the G_{OC} and G_a gates.
2. If $0 < a_{ec2} < 1$, the feedback in the inner loop of G_{OC} gain adjustment becomes negative and ΔG_{OC} can be rewritten as Eq. (51).

$$\Delta G_{oc} = C_2.MO \xrightarrow{Eq.(23)} \Delta G_{oc} = C_2(G_a - G_{oc}).\, SI \tag{51}$$

According to Eq. (51):

2.1. ΔG_{OC} changes are opposite to G_{OC} changes. It is suitable that C_2 and C_1 are chosen small positive values until the gains value of AU and OCU are properly adjusted by the emotional learning mechanism.

2.2. Due to the positive value of the *SI* signal at the initial moment of the operation, the gain value of AU is chosen bigger than the gain value of OCU.

According to the above stability analysis, it is reasonable to choose $C_1 > C_2$, $0 < a_{ec2} < 1$, and $a_{ec1} > a_{ec2}$. Also, it is better to choose the initial value of *SI* coefficients (k_p and k_i) small to allow the intelligent algorithm to determine them correctly. To choose a better initial value of k_p and k_i, the well-known method of Ziegler–Nichols can be used. Also, other coefficients of PI controllers in the control system of the proposed sensor-less DSWIM drive are chosen based on the well-known method of Ziegler–Nichols.

4. Proposed ten-switch inverter for controlling the sensor-less DSWIM drive

Two three-phase motors can be fed separately via a ten-switch converter. This configuration offers a saving of two switches compared to the standard dual three-phase converter structure. Hence, the complexity of this converter is reduced. Fig. 2 shows the plane of the sensor-less DSWIM drive using a ten-switch inverter.

Two three-phase stator winding share the leg C of the converter. Legs A and B in the converter are directly connected to phases $a1$ and $b1$, respectively. Legs D and E are directly connected to phases $a2$ and $b2$, respectively. The function and constraint of switching in this converter are defined as Eqs. (52) and (53), respectively.

$$S_{jm} = \left\{ \begin{array}{l} 1,\ \text{if the switch } S_{jm} \text{ is closed} \\ 0,\ \text{if the switch } S_{jm} \text{ is opened} \end{array} \right\} \tag{52}$$

$$S_{j1} + S_{j2} = 1 \tag{53}$$

where $j =$ A, B, C, D, E is the label of the legs in the ten-switch converter, and $m = 1, 2$ is the number of switches in each leg. A ten-switch converter requires 5 modulation signals ($v_j(t)$, $j =$ A, …, E) to generate switching pulses. There exist 6 modulation signals. Sabarad and Kulkarni (2020) proposed a method as Eq. (54) to decrease the number of signals from 6 to 5.

$$v_i(t) = v_i^*(t) + v_{no}(t) \tag{54}$$

where $i = a, b, c$ and $v_i{}^*(t)$ are major sinusoidal reference signal; $v_{no}(t)$ is zero-sequence signal and does not appear in the line-to-line voltages of the three-phase winding of the stator. In the method proposed by Sabarad and Kulkarni (2020), the modulation signal of the third phase of each winding ($v_{c1}(t)$ and $v_{c2}(t)$) is added to the modulation signals of the other winding phases ($v_k(t)$, $k = a1, b1, a2, b2$), as Eq. (55).

$$v_A(t) = v_{a1}(t) + v_{c2}(t),\ \ v_B(t) = v_{b1}(t) + v_{c2}(t),\\ v_C(t) = v_{c1}(t) + v_{c2}(t),\ \ v_D(t) = v_{a2}(t) + v_{c1}(t),\\ v_E(t) = v_{b2}(t) + v_{c1}(t) \tag{55}$$

$v_{c2}(t)$ has not no effect on the reference voltages of the $abc1$ three-phase winding because it appears as a zero-sequence signal and is cancelled in line-to-line voltages of the $abc1$ three-phase winding. Similarly, $v_{c1}(t)$ has not no effect on the reference voltages of the $abc2$ three-phase winding.

5. Results and discussions

The proposed sensor-less DSWIM drive system is simulated in MATLAB software to consider the proposed models in the different conditions. The parameters of the DSWIM drive are selected from the paper of Guerrero and Ojo (2009) and Munoz (1999). The parameters value of the motor and the proposed control system are presented in Tables B1 and B2, respectively (see Appendix B). The simulation is performed in three models:

1. Conventional DSWIM drive with twelve-switch inverter (CM).
2. Proposed sensor-less DSWIM drive with twelve-switch inverter (PM1).
3. Proposed sensor-less DSWIM drive with the ten-switch inverter (PM2).

In CM, one of the stator windings is generally excited via a constant frequency in the low speed range, and the frequency of the other winding is defined via the demanded speed and torque. When the frequency in one of the windings is fixed at the minimum value (f_{min}), the other stator winding can act in the motor or generator operating mode. Thus, the numerical sum of the torques generated via stator windings must be equal to the demanded torque. In the proposed control method for $T_e > 0$, the total torque is defined as $T_e = T_{e1} + T_{e2} = |T_{e1}| + |T_{e2}|$, although it is defined as $T_e = T_{e1} + T_{e2} \leq |T_{e1}| + |T_{e2}|$ in CM. This issue is the main difference between CM and PMs in producing torque. Fig. 4 shows the performance of CM and PM1 and PM2 at $\omega_r^* = 8rad/s$ with $T_L = 1N.m$. In this study, the first winding in CM is excited via a constant frequency 0.05p.u (f_{min}). The simulation objective in Fig. 4 is to show the performance of CM, PM1, and PM2 in producing the torques (T_{e1} and T_{e2}) and the total rotor flux at a low speed. In Fig. 4(a), it is observed that the PM1 and PM2 perfectly track a low ω_r^* in the transient and steady states. The total electromagnetic torque profile (T_e) is shown in Fig. 4(b), and the torque produced profiles via two stator windings (T_{e1} and T_{e2}) are shown in Fig. 4(c) for all three methods.

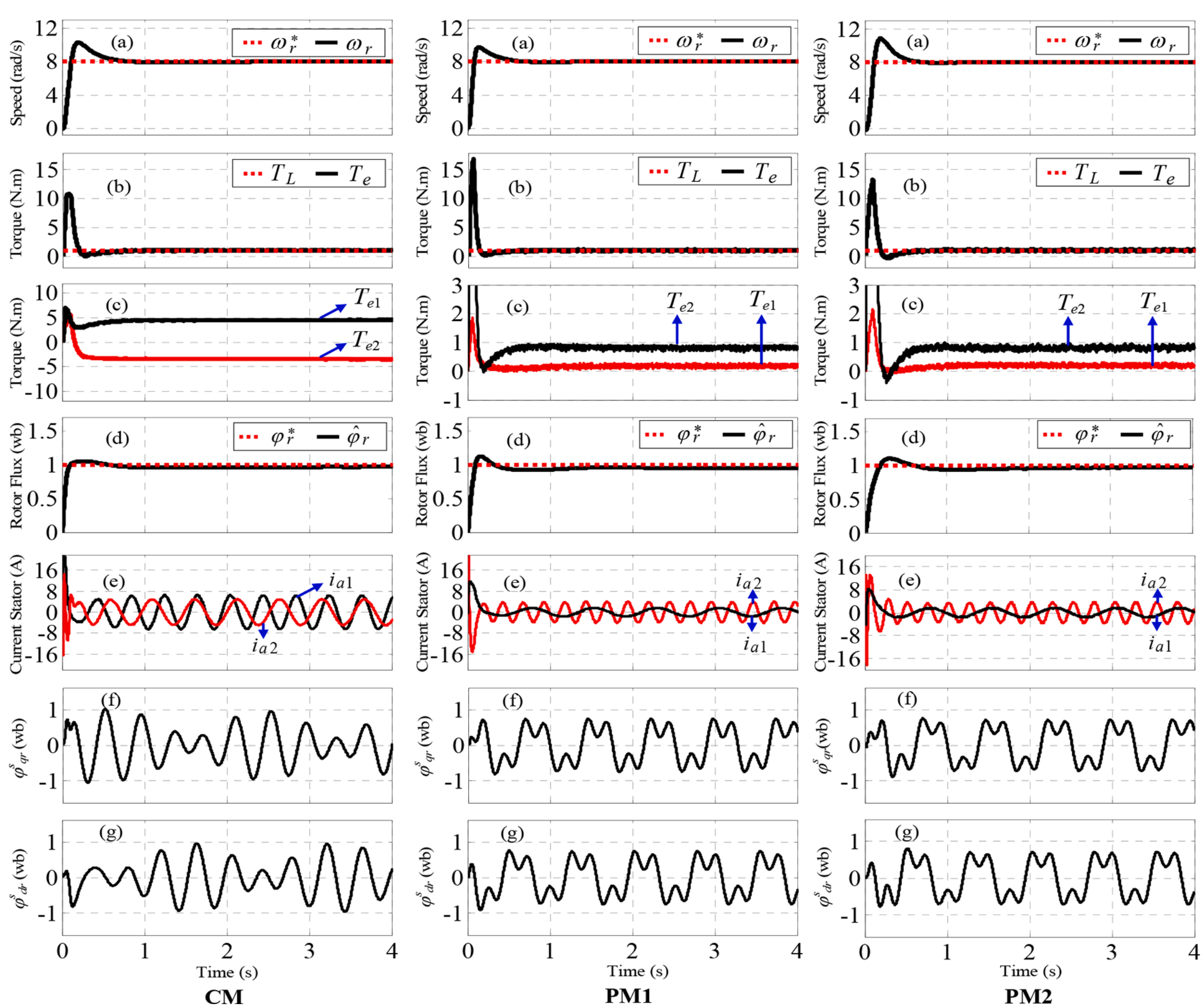

Fig. 4. Simulation results of CM, PM1, and PM2 at $\omega_r^* = 8rad/s$ with $T_L = 1N.m$. a) Speed profile, b) Total torque profile, c) Torque profile in stator windings, d) Total rotor flux, e) Stator currents i_{a1} and i_{a2}, f) q-axis total rotor flux, and g) d-axis total rotor flux.

In the proposed and conventional methods, the sum of generated torques is equivalent to total torque. In CM, one of the stator windings is commonly excited by a constant frequency in the low speed range, and the frequency of other winding is defined via the demanded speed and torque. Thus, one of the stator winding acts as a generator or motor operational mode. As shown in Fig. 4(c), T_{e2} in CM is negative (generator mode) and in PM1 and PM2 is positive (motor mode). In all three methods, the total torque is as $T_e = T_{e1} + T_{e2}$. In two proposed methods, T_{e1} and T_{e2} generated via stator windings are a percentage of T_e that their total percentage does not exceed 100. This issue is a major specification in the normal operational mode of a DSIWM. In Fig. 4(d), it is clear that PM1 and PM2 have an appropriate rotor flux level in the low speed range. PM1 and PM2 well estimate the rotor flux in the transient and steady states as perfectly as CM. Fig. 4(e) shows the first phase current of stator windings. Unlike CM, the models of PM1 and PM2 work in synchronous standard mode. In this mode, the ratio of two frequencies exciting the motor is equal to the pole ratio of 1:3. As a result, the form of the total rotor flux is as nearly trapezoidal (Munoz & Lipo, 2000). In PM1 and PM2, the shape of the rotor flux distribution is trapezoidal as shown in Fig. 4(f) and 4(g), and the motor works in its normal operational mode. But in CM, in the low speed range, the DSWIM works in asynchronous mode. For the conventional method, Fig. 4(f) and 4(g) show the form of the rotor flux distribution is not trapezoidal. The trapezoidal form of the total flux is important because it is expected to improve the stator and rotor iron utilization of the DSWIM.

In this study, three techniques are proposed to improve the accuracy of the speed estimation in the proposed MRAS in the low speed range as follows:

1. The proposed MRAS with the classical PI controller (Technique I).
2. The proposed IMRAS with the single-objective PI controller (Technique II).
3. The proposed IMRAS with the bi-objective PI controller (Technique III).

For $\omega_r^* = 9rad/s$ with $T_L = 2N.m.$, Table 1 shows all three proposed techniques have good accuracy in estimating the speed for Proposed Method 2. The proposed single-objective IMRAS has good accuracy compared to the proposed MRAS with the classical PI controller. But the third proposed technique has good accuracy compared to other techniques in the low speed range. The most important feature of this technique is the information of the reference speed (ω_r^*) involve in the speed estimation calculations by $\Delta\omega_r$. As a result, the convergence between $\widehat{\omega}_r$ and ω_r^* in this technique is increased in the low speed range.

To compare better, Table 2 shows the mean absolute error of the speed estimation between Techniques I and III at zero, very low, and low speeds. As shown it, Technique III has very good accuracy in the low and very low speeds range. In Technique I, k_p and k_i coefficients in the adaptation algorithm are selected based on the Ziegler–Nichols tuning method. This coefficients in all speeds range are constant and are not updated. Also, it is not an optimal method. But, in Technique III, k_p and k_i coefficients in the adaptation algorithm are updated online based on an emotional learning algorithm. Also, Technique III has two objectives ($\xi \to 0$ and $\Delta\omega_r \to 0$) that second objective increases the convergence between estimated speed and reference speed in the proposed IMRAS at zero and very low speeds. According to Table 2, for $\omega_r^* = -0.5rad/s$ with $T_L = 2N.m$, the mean absolute error of the speed estimation of Technique III is very lower than Technique I. At all operating speeds, especially at very low speeds with the light load torque, the performance of Technique III is better than Technique I.

Table 1
Comparison of the absolute error of speed estimation in three proposed techniques for $\omega_r^* = 9rad/s$ with $T_L = 2N.m.$

Technique No.	Absolute error of speed estimation (rad/s)		
	Min	Max	Mean
I	0.0892	0.1175	0.1041
II	0.0394	0.0769	0.0585
III	2.2469×10^{-6}	0.0133	0.0036

Table 2
Mean absolute error of the speed estimation in Techniques III and I at different operations.

Speed (rad/s)	Load torque (N.m)	Mean absolute error of speed estimation (rad/s)	
		I	III
0	4	0.3586	0.0014
5	4	0.1247	0.0047
8	4	0.1395	0.0015
−0.5	2	0.3956	7.8021×10^{-4}
−3	2	0.1672	0.0046
−9	2	0.1021	0.0039

Fig. 5 shows the simulation results of Proposed Method 2 for the rated load torque. In Fig. 5(I) and 5(II), the reference speed change from −1 to 1 rad/s and from −5 to 5 rad/s, respectively. As shown in Fig. 5 (a), PM2 well traces low speeds in the transient and steady states. The total torque profile (T_e) is shown in Fig. 5(b). Fig. 5(c) and 5(d) show three-phase currents of stator windings (i_{abc1} and i_{abc2}). In PM2, R_r associates in estimating d– and q–axis rotor fluxes in the adaptive model of the IMRAS. For $\omega_r^* = 9rad/s$ with $T_L = 2N.m.$, Fig. 6 shows the simulation results of PM2 for 0 to 90 % changes in R_r. Fig. 6($a_{1\text{-}4}$) shows the estimated and actual speeds profile. As seen in these figures, the proposed intelligent sensor-less DSWIM drive traces well the low speeds in the transient and steady states. Fig. 6(c) shows the normalized sensitivity functions of $\widehat{\varphi}_{dr}^s$ and $\widehat{\varphi}_{qr}^s$ to R_r changes in the adaptive model of IMRAS that $S_{R_{r1}}^{\widehat{\varphi}_{dr}^s}$ and $S_{R_{r1}}^{\widehat{\varphi}_{qr}^s}$ are less than 4 %. Fig. 6(d) and 6(e) show d– and q–axis estimated rotor flux for 0, 30, 60 and 90 % variations in R_r, respectively. In the proposed adaption algorithm, the k_p and k_i coefficients values are modified and updated with changing R_r. From Fig. 6, it is obvious that PM2 has appropriate robustness to changes of R_r in the low speed range. The important feature of the IMRAS is its minor sensitivity to changes in R_r.

Fig. 7(a) shows steady-state current of the legs in the ten-switch converter of PM2 for $\omega_r^* = 40rad/s$ with $T_L = 3N.m$, and also Fig. 7(b) shows the related spectrum to legs current. As seen from the current spectrum in Fig. 7(b), the leg C current includes two sinusoidal components its lower and higher frequency belongs to the third phase of the $abc1$ and $abc2$ windings (i_{c1} and i_{c2}), respectively. PM2 has two important features compared to PM1 and CM:

1. In PM2, two IGBT/Diode units are saved to decrease the cost of the converter.
2. PM2 has lower power losses of the inverter compared to CM and PM1.

For the second feature, Fig. 8 shows the simulation results of CM, PM1, and PM2 for $\omega_r^* = 8rad/s$ with $T_L = 1N.m.$ Fig. 8(a) shows the sum of total power losses of switching and conducting in the converter of the DSWIM drive for CM, PM1, and PM2. The proposed methods have a significant decrease in losses compared to CM. In the proposed and conventional methods, the numerical sum of generated torques is equivalent to the total torque. In CM, it is feasible for one of the stator windings to generate torque greater than the total torque. In PM1 and PM2, the generated torque via each stator winding is constantly smaller than the total torque. Hence, it is expected to be improved the ratio of T/I and to be reduced the total power losses in the converter of PM1 and PM2 compared to CM. As shown in Fig. 8(b), PM1 and PM2 have a better ratio of T/I than CM. As stated by Guerrero and Ojo (2009), to have a proper ratio of T/I in the DSWIM drive, it must operate in its normal operational mode.

The main purpose of the proposed DSWIM drive system is to control the rotor speed. Therefore, in second revised manuscript, the proposed

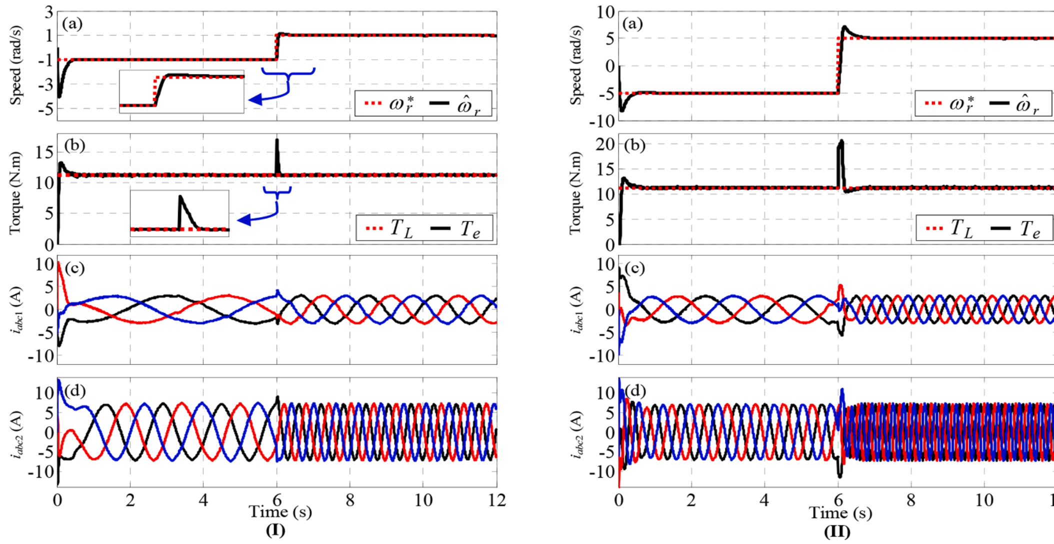

Fig. 5. Simulation results of PM2 in the low speed ranges of ± 1 rad/s and ± 5 rad/s in rated load torque. a) Speed profile, b) Total electromagnetic torque profile, and c, d) Stator currents of stator windings (i_{abc1}, i_{abc2}).

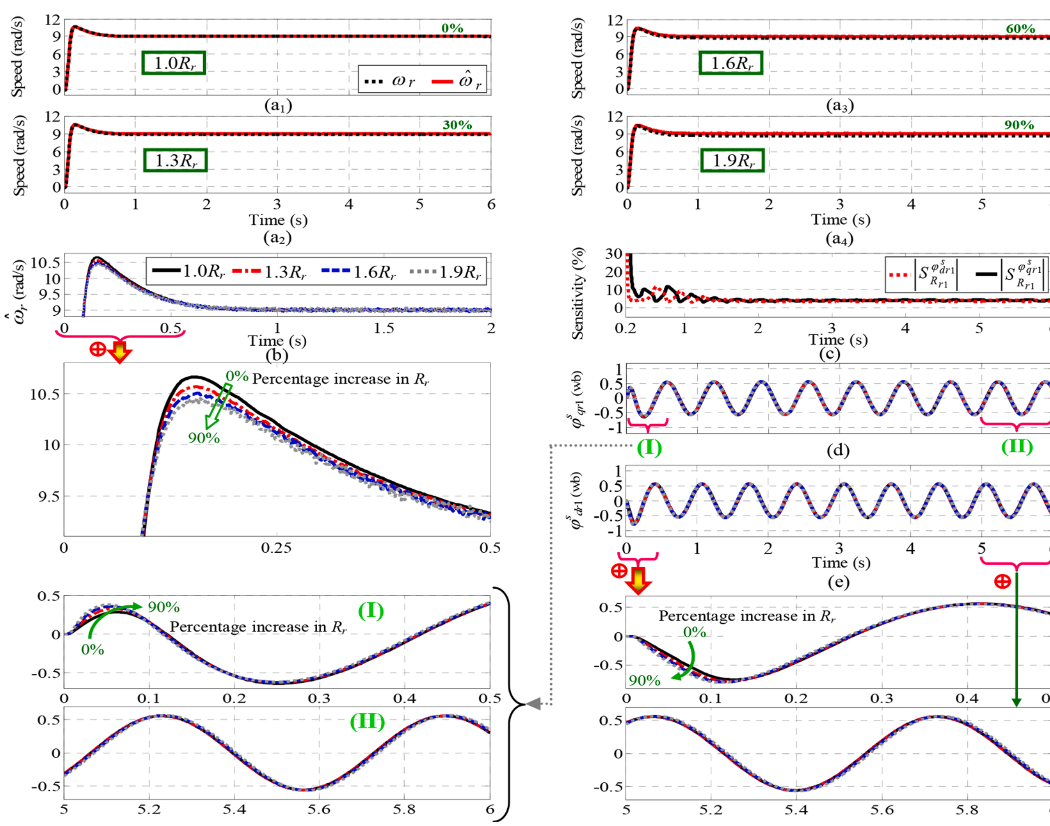

Fig. 6. Simulation results of PM2 for 0 to 90 % variations in rotor resistance in response to $\omega_r^* = 9rad/s$ with $T_L = 2N.m$: a₁₋₄) Estimated and actual speeds profiles for 0, 30, 60 and 90 % variations in rotor resistance, b) Estimated speed profiles for 0 to 90 % changes in R_r, c) Normalized sensitivity functions of $\hat{\varphi}^s_{dr}$ and $\hat{\varphi}^s_{qr}$ to R_r changes ($S^{\hat{\varphi}^s_{dr}}_{R_{r1}}$ and $S^{\hat{\varphi}^s_{qr}}_{R_{r1}}$), and d, e) d– and q–axis estimated rotor flux for 0, 30, 60 and 90 % variations in rotor resistance.

method is tested in its most difficult test which is a highly variable step command at low speeds. Fig. 9 shows the behavior of the proposed method at the step speed command of 2-4-6-8-10-8-6-4-2-0-(-2)-(-4) rad/s and in time intervals 0-0.3-0.6-0.9-1.2-1.5-1.8-2.1-2.4-2.7-3-3.3-3.6 s and with a constant load torque of 1 N.m. As seen in this figure, the sensor-less DSWIM drive tracks the actual rotor speed very well. The step reference speed is tracked favorably from the point of view of the transient and steady state.

Table 3 presents a comparison of the reduction percentage of the total power losses among CM, PM1 and PM2 for $\omega_r^* = 0, 0.4, 2, 8,$ *and* $8rad/s$ with $T_L = 2, 8, 3, 1,$ *and* $5N.m$, respectively. According to this table, it is clear that PM1 has lower power losses than CM in very low speed regions with light loads and the loss reduction is significant. In PM1, the generated torque of each winding is constantly lower than the

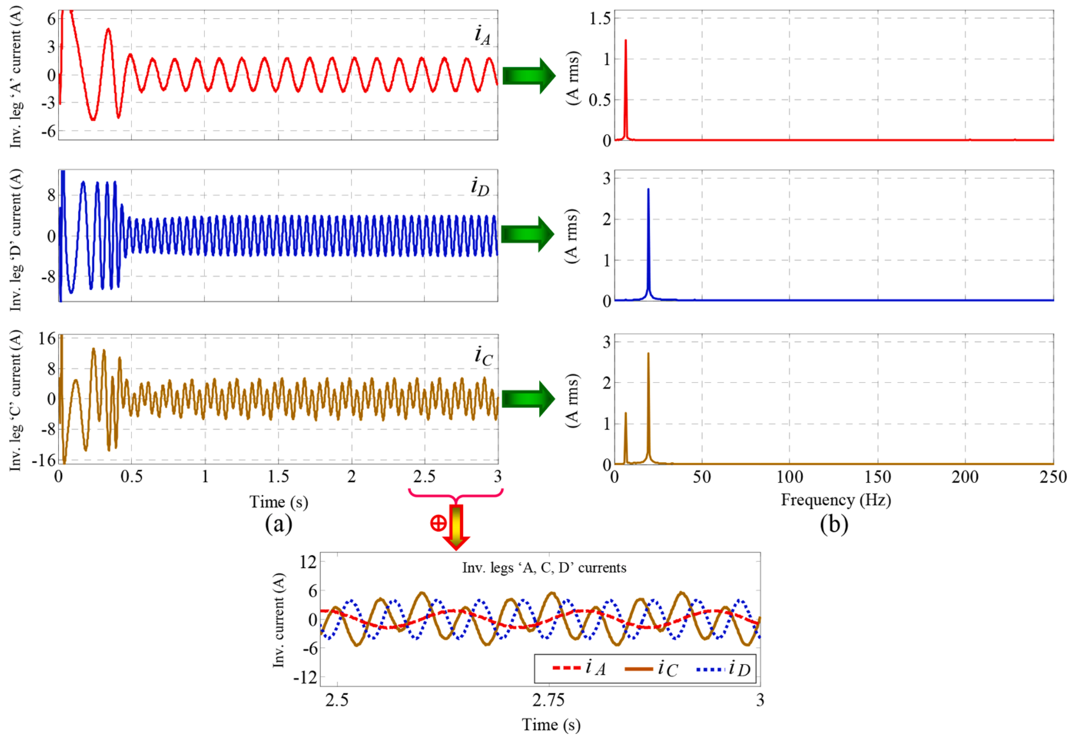

Fig. 7. Steady-state current of the Legs in the ten-switch converter of PM2 and the related spectrum to legs current for $\omega_r^* = 40rad/s$ with.$T_L = 3N.m$.

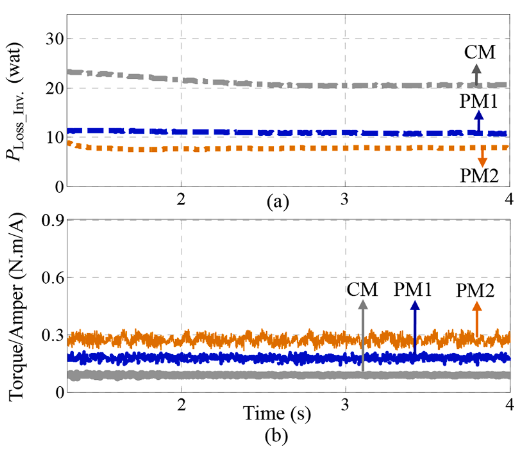

Fig. 8. Simulation results of CM, PM1, PM2 for $\omega_r^* = 8rad/s$ with $T_L = 1N.m$: a) Sum of the total power losses (containing conducting and switching losses) in the converter and b) Torque per ampere ratio.

total torque. It is clear in Fig. 4(b) that the total T_e is 1 N.m, but T_{e1} is more than T_e because its excitation frequency is fixed at 0.05p.u. In PM2, two switches are saved compared to CM, and also the total power losses of the inverter are reduced as observed in Table 3.

Table 4 presents a comparison between the proposed sensor-less DSWIM drive (PM2) and the conventional DSWIM drive (CM). In the proposed method, unlike conventional methods, the form of the total rotor flux is as trapezoidal and the rotor speed is estimated in the low speed range and the DSWIM drive work in its standard mode. In addition, two IGBT/Diode units are saved compared to the conventional method.

As the result of the analysis, the proposed methods control the rotor flux and speed of a DSWIM based on intelligent ideas and a ten-switch converter in low speed range. The obtained analysis results are organized as follows:

1. The intelligent proposed sensor-less DSWIM drive, unlike conventional methods, works in its standard operating mode (synchronous mode) and has a suitable performance in the low speed range.
2. The proposed intelligent speed estimator has very good accuracy in the low and very low speeds ranges.
3. As the result of the analysis, in the proposed inverter unit, the total power losses of the inverter are reduced as observed in Table 3, and also two switches are saved compared to the conventional method.

6. Conclusions

This paper presented modeling of single and bi-objective brain emotional intelligent controllers to improve the performance of a sensor-less DSWIM drive. The main purpose of this study was to maintain the normal operational mode of a sensor-less DSWIM drive, unlike the conventional method, using an intelligent structure, and also a ten-switch inverter in low speed range. In this study, the following three proposed issues were considered:

Step 1. The rotor flux is compensated to solve the issue of the low rotor flux in the low speed range without estimating R_s, and also decreased power losses in the converter.

Step 2. The novel IMRAS is proposed to estimate the rotor speed, in the low speed range.

Step 3. In the proposed methods, two IGBT/Diode units are saved compared to the conventional method, and also the total power losses of the inverter are reduced.

In this manuscript, the advantages of the proposed sensor-less DSWIM drive compare to other approaches were as following cases:

1. In all operating speeds, especially at low speeds, the proposed sensor-less DSWIM drive is operated in its standard operating mode (synchronous mode).
2. The new intelligent model reference adaptive system (IMRAS) is proposed to estimate the rotor speed in the proposed DSWIM drive system via the proposed ideas in the low speed range that the drive is controlled in the synchronous mode.

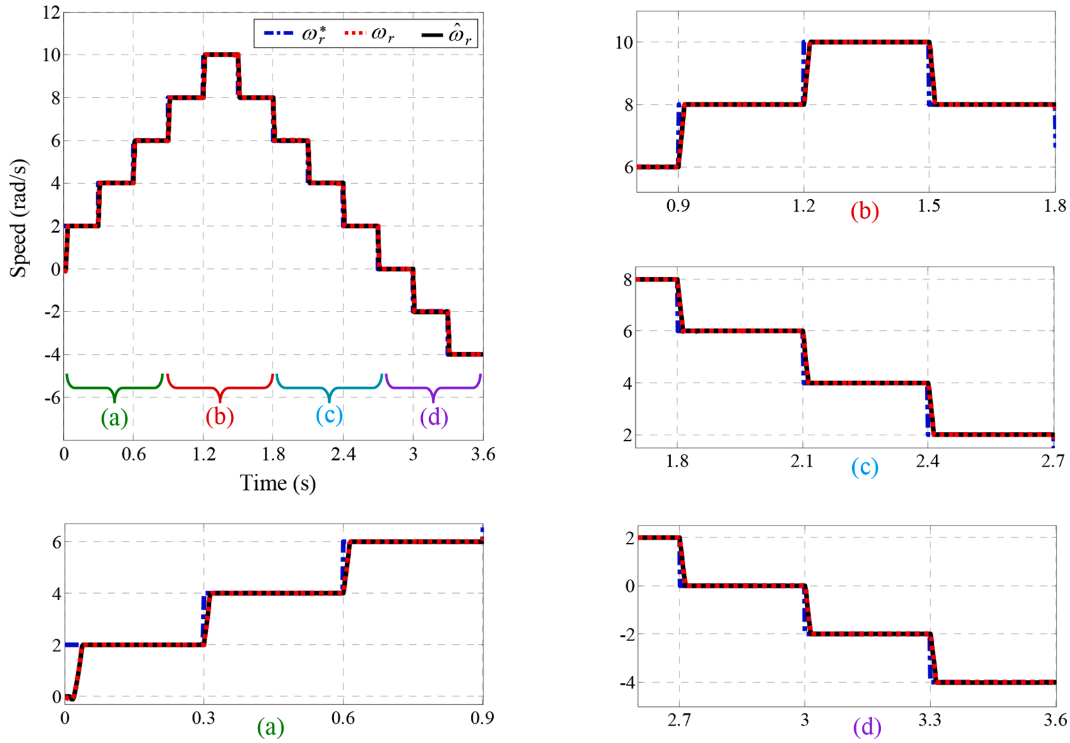

Fig. 9. Speed profile of the proposed method at step speed command with $T_L = 1$ *N.m.*

Table 3
Comparison of reduction percentage of total power losses in the converter among CM, PM1, and PM2.

Speed (rad/s)	Load torque (N.m.)	Reduction of total power losses in the converter (in %)		
		PM1 compared to CM	PM2 compared to CM	PM2 compared to PM1
0	2	69.13	71.46	07.54
0.4	8	43.94	50.28	10.82
2	3	54.46	62.85	18.42
8	1	47.81	61.5	26.23
8	5	22.51	27.52	06.46

Table 4
Comparison between the proposed sensor-less DSWIM drive (PM2) and the conventional DSWIM drive (CM).

Method	Rotor speed Estimation in the standard mode at low speeds	Number of inverter switches	Trapezoidal total rotor flux (standard mode)
Proposed DSWIM drive (PM2)	✓	10	✓
Conventional DSWIM drive (CM)	×	12	×

3. In the proposed methods, two IGBT/Diode units are saved compared to the conventional method, and also the total power losses of the inverter are reduced. The ten-switch converter has the advantages of small size and low cost.

The relationship between above three steps is shown in Fig. 10. The proposed methods controlled the rotor flux and speed of a DSWIM based on intelligent ideas and a ten-switch converter in low speed range.

For future works on this research, it is suggested two cases: 1. Robusting control system to reach the proper performance for the motor parameters variation and adjusting loops controllers coefficients online; and 2. It is suitable to be considered in future research from the natural attribute of the drive to work as a dual voltage generator. This is a very good characteristic for certain applications especially those related to the transportation industry.

CRediT authorship contribution statement

Hojat Moayedirad: Writing – original draft, Conceptualization, Resources, Formal analysis, Writing – review & editing, Investigation, Software, Validation. **Mohammad Ali Shamsi-Nejad:** Supervision.

Declaration of competing interest

The authors declare that they have no known competing financial interests or personal relationships that could have appeared to influence the work reported in this paper.

Data availability

No data was used for the research described in the article.

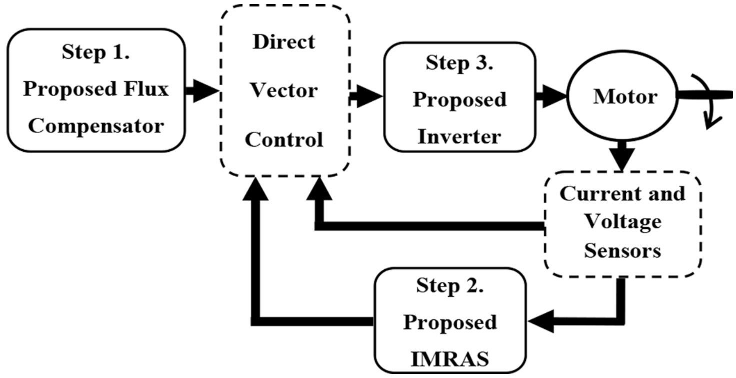

Fig. 10. The block diagram of the proposed research.

Appendix A

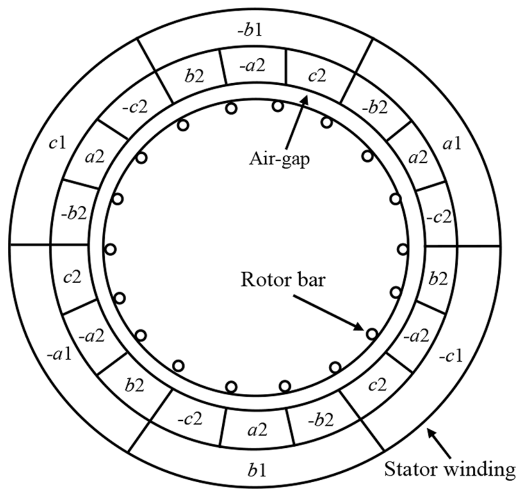

Fig. A1. A shape of the dual stator winding of the DSWIM with the 2-pole and 6-pole windings.

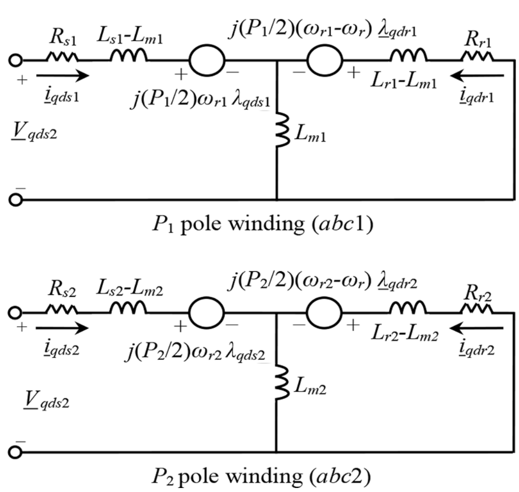

Fig. A2. The equivalent circuit of the DSWIM (Munoz & Lipo, 2000).

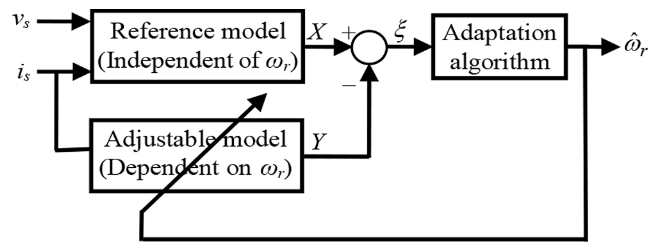

Fig. A3. Basic scheme of the model reference adaptive system.

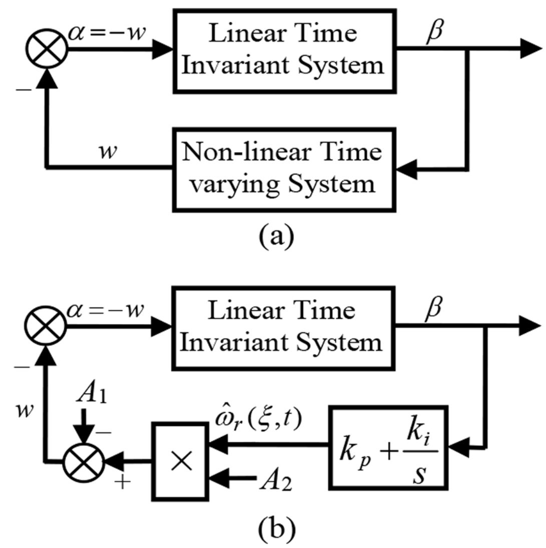

Fig. A4. a) Nonlinear feedback system, b) Equivalent structure of the proposed method.

Appendix B

Tables B1 and B2 show the value of the parameters in the sensor-less DSWIM drive, where P_n and f_n are the rated power and frequency of the motor; f_{sw} is the switching frequency in the inverters; R_b and R_e are rotor bar and end ring resistance, respectively; J is moment of inertia; L_b and L_e are rotor bar and end ring inductance, respectively, and also L_{lr1} and L_{lr2} are rotor leakage inductances.

Table B1
Parameters of the DSWIM drive (Guerrero & Ojo, 2009; Munoz, 1999).

Parameter	value	Parameter	value	Parameter	value	Parameter	value
P_n	2 hp	L_{lr1}	0.006 H	R_{r2}	0.55 Ω	$K_{p1} = 0.5$	$K_{i1} = 0.16$
f_n	60 Hz	L_{lr2}	0.009 H	K_1	0.186	$K_{p2} = 1.1$	$K_{i2} = 0.17$
P_2:P_1	6:2	L_{m2}	0.093 H	f_{min}	3 Hz	$K_{p3} = 40$	$K_{i3} = 0.1$
R_{s1}	3.4 Ω	R_{s2}	1.9 Ω	K_2	0.662	$K_{p4} = 1$	$K_{i4} = 2.5$
L_{ls1}	0.006H	L_{ls2}	0.009 H	f_{sw}	5 kHz	$K_{p5} = 80$	$K_{i5} = 0.1$
R_{r1}	0.61 Ω	L_{m1}	0.336 H	J	0.1 Kg-m^2	$K_{p6} = 0.73$	$K_{i6} = 1.5$
R_e	0.16 µΩ	R_b	47 µΩ	L_e	15 nH	$K_{p7} = 5.6$	$K_{i7} = 0.9$
L_b	82 nH	–	–	–	–	–	–

Table B2
Parameters of the proposed IMRAS.

Parameter	value	Parameter	value
a_{ec1}	27	C_2	0.1
a_{ec2}	0.7	k_p	2.6
a_{ec3}	2.7	k_i	1.4
C_1	1	–	–

References

Adamczyk, M., & Kowalska, T. O. (2022). Postfault direct field-oriented control of induction motor drive using adaptive virtual current sensor. *IEEE Transactions on Industrial Electronics, 69*(4), 3418–3427. https://doi.org/10.1109/TIE.2021.3075863

Blanchard, E., Blaszczyk, L., Deprez, T., Franzl, N., & Dupuy, A. (2009). Mediators of hedonic regulation of food intake. *Retrieved from the Database Center for Life Science (DBCLS) at*.

Bose, B. K. (2002). *Modern power electronics and AC drives*. New Jersey, NJ, USA: Upper Saddle River.

Choi, D., Lee, J. S., Lim, Y. S., & Be, K. B. (2023). Priority-based model predictive control method for driving dual induction motors fed by five-leg inverter, *IEEE Transactions on Power Electronics, 38*(1), 887–900. https://doi.org/ 10.1109/TPEL.2022.3203961.

Farshad, M., & Lucas, C. (2006). *Modeling, design and intelligent control of switched reluctance motor (SRM) for washing machine application*. Ph.D. dissertation. Tehran, Iran: University of Tehran.

Geng, Q., Li, Z., Zhang, M., Zhou, Z., Wang, H., & Shi, T. (2022). Sensorless control method for dual permanent magnet synchronous motors driven by five-leg voltage source inverter. *IEEE Journal of Emerging and Selected Topics in Power Electronics, 10* (1), 260–272. https://doi.org/10.1109/JESTPE.2021.3096198

Guerrero, J. M., & Ojo, O. (2009). Total air gap flux minimization in dual stator winding induction machines. *IEEE Transactions on Power Electronics, 24*(3), 787–795. https://doi.org/10.1109/APEC.2008.4522864

Hu, J., & Wu, B. (1998). New integration algorithms for estimating motor flux over a wide speed range, *IEEE Transactions on Power Electronics, 13*(5), 969–976. https://doi.org/ 10.1109/63.712323.

Jing, G., & Zhou, Ch. (2020). Control strategy for a five-leg inverter supplying dual three-phase PMSM. *IEEE Access, 8*, 174480–174488. https://doi.org/10.1109/ACCESS.2020.3025392

Kowalska, T. O., & Dybkowski, M. (2010). Stator-current-based MRAS estimator for a wide range speed-sensorless induction-motor drive. *IEEE Transactions on Industrial Electronics, 57*(4), 1296–1308. https://doi.org/10.1109/TIE.2009.2031134

Kumar, P., & Hati, A. S. (2022). Dilated convolutional neural network based model for bearing faults and broken rotor bar detection in squirrel cage induction motors. *Expert Systems with Applications, 191*, Article 116290. https://doi.org/10.1016/j.eswa.2021.1162902

Landau, Y. P. (1979). *Adaptive control: The model reference approach*. New York: Marcel Dekker.

Luo, C., Wang, B., Yu, Y., Chen, C., Huo, Z., & Xu, D. (2020). Decoupled stator resistance estimation for speed-sensorless induction motor drives considering speed and load torque variations. *IEEE Journal of Emerging and Selected Topics in Power Electronics, 8* (2), 1193–1207. https://doi.org/10.1109/JESTPE.2019.2915969

Mahato, B., Majumdar, S., & Jana, K. Ch. (2020). Reduction of power electronic devices in a single-phase generalized multilevel inverter, *Journal of Circuits, Systems, and Computers*, *29*(6), 2050093(1-25). https://doi.org/10.1142/S0218126620500930.

Moayedirad, H., Farshad, M., & Shamsi-Nejad, M. A. (2012). Improvement of speed profile in induction motor drive using a new idea of PWM pulses generation base on artificial neural networks. *Computational Intelligence in Electrical Engineering, 2*(4), 35–46.

Moayedirad, H., Shamsi-Nejad, M. A., & Farshad, M. (2011). Neural control of the induction motor drive: Robust against rotor and stator resistances variations and suitable for very low and high speeds. *Iranian Journal of Electrical and Computer Engineering, 9*(2), 107–113.

Moayedirad, H., Shamsi-Nejad, M. A., & Farshad, M. (2012). Improvement of induction motor drive operation in low and high speeds using rotor flux compensation. *Journal of Iranian Association of Electrical and Electronics Engineers, 9*(2), 59–64.

Moaveni, B., Masoumi, Z., & Rahmani, P. (2023), Introducing improved iterated extended Kalman filter (IIEKF) to estimate the rotor rotational speed, rotor and stator resistances of induction motors, *IEEE Access*, *11*, 17584–17593. https://doi.org/10.1109/ACCESS.2023.3244830.

Munoz, A. R. (1999). *Analysis and control of a dual stator winding squirrel cage induction machine*. Ph.D. dissertation. Madison: University of Wisconsin.

Munoz, A. R., & Lipo, T. A. (2000). Dual stator winding induction machine drive. *IEEE Transactions on Industry Applications, 36*(5), 1369–1379. https://doi.org/10.1109/28.871286

Moren, J., & Balkenius, C. (2000, October). A Computational Model of Emotional Learning in the Amygdala, In *Proceedings of the Sixth International Conference on the Simulation of Adaptive Behavior*, Paris.

Novotny, D. W., & Lipo, T. A. (1997). *Vector control and dynamics of AC drives*. New York, USA: Oxford University Press Inc.

Ojo, O., & Wu, Z. (2008). Modeling of a dual-stator-winding induction machine including the effect of main flux linkage magnetic saturation, *IEEE Transactions on Industry Applications, 44*(4), 1099–1107. https://doi.org/ 10.1109/TIA.2008.926058.

Ojo, O., & Wu, Z. (2007, February). Speed control of a dual stator winding induction machine. In *Twenty-Second Annual IEEE Applied Power Electronics Conference and Exposition*, Anaheim, CA, USA, 229–235. https://doi.org/10.1109/APEX.2007.357519.

Özkurt, G., & Zerdali, E. (2022). Design and implementation of hybrid adaptive extended Kalman filter for state estimation of induction motor. *IEEE Transactions on Instrumentation and Measurement, 71*, 1–12. https://doi.org/10.1109/TIM.2022.3144729

Reddy, S. R. P., & Loganathan, U. (2022). Adaptation of slip gain for modified transient vector estimator-based speed control of induction machine drive". *IEEE Journal of Emerging and Selected Topics in Power Electronics, 10*(1), 248–259. https://doi.org/10.1109/JESTPE.2021.3115095

Reddy, C. U., Prabhakar, K. K., Singh, A. K., & Kumar, P. (2020). Speed estimation technique using modified stator current error-based MRAS for direct torque controlled induction motor drives. *IEEE Journal of Emerging and Selected Topics in Power Electronics, 8*(2), 1223–1235. https://doi.org/10.1109/JESTPE.2019.2901523

Rouhani, H., Jalili, M., Araabi, B. N., & Eppler, w., & Lucas, C.. (2007). Brain emotional learning based intelligent controller applied to neurofuzzy model of micro-heat exchanger. *Expert Systems with Applications, 32*(3), 911–918. https://doi.org/10.1016/j.eswa.2006.01.047

Sabarad, J., & Kulkarni, G. H. (2020). Novel switching technique for five leg inverter in dual motor control. *Indonesian Journal of Electrical Engineering and Computer Science, 19*(2), 644–651. https://doi.org/10.11591/ijeecs.v19.i2

Savarapu, S., Qutubuddin, M., & Narri, Y. (2022). Modified brain emotional controller-based ripple minimization for SVM-DTC of sensorless induction motor drive. *IEEE Access, 10*, 40872–40887. https://doi.org/10.1109/ACCESS.2022.3165651

Schauder, C. (1992). Adaptive speed identification for vector control of induction motors without rotational transducers. *IEEE Transactions on Industry Applications, 28*(5), 1054–1061. https://doi.org/10.1109/28.158829

Shamsi-Nejad, M. A., Farshad, M., & Moayedirad, H. (2010, June). A new method of PWM pulses generation in induction motor drive using artificial neural networks, *SPEEDAM 2010*, Pisa, Italy, 942–946.

Stender, M., Wallscheid, O., & Bocker, J. (2021). Accurate torque control for induction motors by utilizing a globally optimized flux observer, *IEEE Transactions on Power Electronics, 36*(11), 13261–13274. https://doi.org/ 10.1109/TPEL.2021.3080129.

Sun, J., Li, C., Zheng, Z., Wang, K., & Li, Y. (2021). Online estimation of per-phase stator resistance based on DC-signal Injection for Condition monitoring in multiphase drives. *IEEE Transactions on Industrial Electronics, 69*(3), 2227–2239. https://doi.org/10.1109/TIE.2021.3066935

Wang, W., Lu, Z., Hua, W., Wang, Z., & Cheng, M. (2020). Dual-level located feedforward control for five-leg two-mover permanent-magnet linear motor traction systems. *IEEE Transactions on Power Electronics, 35*(12), 13673–13686. https://doi.org/10.1109/TPEL.2020.2995241

Wang, H., Yang, Y., Xinglai, G., Zuo, Y., Yue, Y., & Songtao, L. (2022). PLL- and FLL-based speed estimation schemes for speed-sensor-less control of induction motor drives: Review and new attempts. *IEEE Transactions on Power Electronics, 37*(3), 3334–3356. https://doi.org/10.1109/TPEL.2021.3117697

Wu, Z., Ojo, O., & Sastry, J. (2007). High-performance control of a dual stator winding DC power induction generator. *IEEE Transactions on Industry Applications, 43*(2), 582–592. https://doi.org/10.1109/TIA.2006.890020

Yildiz, R., Barut, M., & Zerdali, E. (2020). A comprehensive comparison of extended and unscented Kalman filters for speed-sensor-less control applications of induction motors. *IEEE Transactions on Industrial Informatics, 16*(10), 6423–6432. https://doi.org/10.1109/TII.2020.2964876

Yoo, J., Lee, J., Sul, S., & Baloch, N. A. (2020). Stator resistance estimation using DC injection with reduced torque ripple in induction motor sensor-less drives. *IEEE Transactions on Industry Applications, 56*(4), 3744–3754. https://doi.org/10.1109/TIA.2020.2984189

Zerdali, E. (2020). A comparative study on adaptive EKF observers for state and parameter estimation of induction motor. *IEEE Transactions on Energy Conversion, 35* (3), 1443–1452. https://doi.org/10.1109/TEC.2020.2979850

Zhao, H., Eldeeb, H. H., Wang, J., Kang, J., Zhan, Y., Xu, G., & Mohammed, O. A. (2021). Parameter identification based online noninvasive estimation of rotor temperature in induction motors. *IEEE Transactions on Industry Applications, 57*(1), 417–426. https://doi.org/10.1109/TIA.2020.3039940